KSCE Journal of Civil Engineering (0000) 00(0):1-15

DOI 10.1007/s12205-015-1529-z

Geotechnical Engineering

pISSN 1226-7988, eISSN 1976-3808
www.springer.com/12205

Field Testing and Analysis During Top-down Construction of Super-tall Buildings in Shanghai

Yongjing Tang* and Xihong Zhao**

Received September 11, 2014/Revised 1st: January 13, 2015, 2nd: March 20, 2015/Accepted May 4, 2015/Published Online June 12, 2015

Abstract

Although certain measurements regarding super-tall buildings constructed using the top-down method have been published, new advances in top-down construction have been developed with the construction of super-tall buildings in China. This paper presents the theory of soil-structure interactions in pile foundations and extends it to the top-down construction method. Based on this theory, the forces and the deformation of the diaphragm wall, slab and soldier piles at various stages of construction can be computed. Two typical tall buildings of 60 and 37 stories with deeply embedded 4-level and 5-level basements located in Shanghai were used as case studies of the vertical displacements of their diaphragm walls and soldier piles, the deflections of the diaphragm walls, the earth pressures, and the rebar stresses during top-down construction. The values measured in the field agree well with the predicted values from soil-structure interactions theory and statistical-empirical formulas. Two additional super-tall buildings of 101 and 121 stories, in which the 4-level and 5-level basements and the main buildings are round, are discussed regarding their unique deformational characteristics. In addition, the diaphragm wall can serve a load-sharing function. These engineering case studies, including the comprehensive predictions of deformation based on field tests and estimates using statistical formulas, can improve tall building design.

Keywords: *top-down method, deep excavation engineering, deflection, heave, differential deformation*

1. Introduction

The concept of top-down construction was first used in Japan to shorten construction schedules. In 1935, this technique was used to construct a building founded in a dry excavation in Tokyo (Wang, 2011). In the 1950s, the Italian (Milan) company ICOS further developed the Top-down Method (TDM) by combining a diaphragm wall with the TDM in an excavation in the presence of shallow groundwater. Subsequently, TDM has been used worldwide, particularly in Asia. In the USA, Cotton and Luark (2010) analyzed recent advances in the TDM with the use of a 26.4-m-tall soil-nail retention system. That project involved several innovative techniques, including the construction of the permanent building wall from the top to down, thereby eliminating the need for temporary shoring. These innovative techniques resulted in significant cost savings. Kudsk *et al.* (2013) concluded that the manufacturing industry has made great improvements in efficiency and cost reductions during the previous few centuries, but the same improvements have not occurred in the construction industry, based on a study of one of the largest construction companies in Northern Europe. Modularization in the construction industry using the TDM may be one potential source of improvement. In South Korea, Lee *et al.* (1999) proposed a non-shored TDM formwork system. The advantages of this system include a reduction in excavation duration and an improvement in the quality of underground concrete work by use of hanging-type formwork. A case study was performed to verify the validity. Based on a bottom-up pile load test, Kim and Mission (2011) presented an improved evaluation of the equivalent load-displacement curve during TDM construction, which indicated that this curve agreed with the measured and simulated top-down curves, as validated in the case studies. In Korea, Rhim *et al.* (2012) developed an optimum pre-formed column system for the TDM. The circular concrete-filled tubular steel columns are preferred over the more popular H-shaped columns. Such columns combined with a well-developed shear connection system were applied to an actual top-down construction process. This column system is considered to have good constructability characteristics and is effective in reducing the construction costs and time.

In Shanghai, one of the world's most densely populated cities, we used the TDM to minimize the deflection of the diaphragm wall and create extra working space during building construction. In 1983, a 5-story building with a 2-story basement became the first building to use the TDM in Shanghai. In China, the theory behind the TDM was studied for the first time as part of two PhD

*Associate Professor, PE, Key Laboratory of Geotechnical and Underground Engineering, Ministry of Education; Dept. of Geotechnial Engineering, Tongji University, Shanghai 200092, China (Corresponding Author, E-mail: ytang@tongji.edu.cn)
**Professor; Dept. of Geotechnial Engineering, Tongji University, Shanghai 200092, China (E-mail: xihongzhaocn@126.com)

dissertations. The first study by Tang (1996) presented the key factors affecting differential settlement among the diaphragm wall and soldier piles. In the second study by Tang (1996) concluded that the diaphragm wall can also act as the loading wall. These two innovative studies created a basis for the use of the TDM in China. Zhao (1999) firstly incorporated the theory of superstructure-foundation interactions into the practice of TDM construction. Xu and Zhao (2003) systematically presented the theory, method and construction technique. Meanwhile, the technique has been used in more than 30 projects in China. Kung (2009) analyzed how wall deflections are affected by the excavation depth, strut stiffness, and creep during the placement of the floor slab. Kung (2009) also summarized 26 excavation case histories involving Taipei's silty clay regarding wall deflection caused by the TDM and bottom-up method (BUM) and compared these methods. These results of these observation and comparison are valuable.

Recently, Wang (2011) summarized construction experience, including soldier pile construction techniques and excavation designs to ensure structural safety, with the TDM in Shanghai and throughout China, where the TDM is widely used. Jia *et al*. (2012) described their analysis and design of the 121-story Shanghai Center Tower (SCT) and 37-story podium using the TDM. Wang (2014), based on measured and analyzed results, explained the deformation characteristics of the SCT podium pit and analyzed the basement excavation technique. These two papers provide good descriptions of the use of TDM in constructing the SCT. Tan and Wang (2013) described the characteristics of the foundation excavation for the 101-story Shanghai World Financial Center (SWFC), which was constructed using the TDM. Zhao *et al.* (2014) wrote a book, "Comprehensive Study on a Field Experiment for the Piled Raft Foundation of the 101-storey Shanghai World Financial Centre", in which the wall deflection and heave are analyzed.

The design and construction of the 121-story SCT and the 101-story SWFC are still being investigated. This SCT project involves a circular diaphragm wall retaining system with a diameter of 123 m and an embedment depth of 31.4 m. The SWFC project involves a circular diaphragm wall retaining system with an embedment depth of 18.45 m.

Tan and Li (2011) reported the results of field testing associated with the TDM during construction of the Shanghai subway. The measured data, which involved a 26-m excavation for the subway station, were presented.

The construction of super-tall buildings in soft soil areas poses great challenges with regard to deeper basements, stricter requirements for the displacement of adjacent buildings and smaller operational space during construction. The TDM addresses these challenges very effectively and presents unique advantages.

In order to further prove the theory of soil-structure interaction which had been used in TDM and BUM (Zhao, 1999) combing with the statistical-empirical formulas, experienced over decades, in this paper two case studies of podium construction, focusing on two typical tall buildings with deep basements in Shanghai: the 60-story Chang-feng Market (CFM),which has a 10-story podium, a 4-level basement, and an embedment of 18.94 m; and the 37-story Liao-chuang-xing Financial Center (LCXFC), which has a 3-story podium, a 5-level basement, and an embedment of 22.4 m. The differential vertical displacements between the diaphragm walls and a soldier pile and two adjacent soldier piles are described and analyzed. Zhao *et al.* (1999) compared the computed results with the measured results by real engineering projects to prove the feasibility and validity of the theory of soil-structure interaction and to demonstrate that the special characteristics of the TDM are superior to those of the BUM. However, the differential deformation between diaphragm wall and adjacent soldier pile is still large problem during construction. In addition, the diaphragm wall can also serve a load-sharing function.

The second author participated in the field testing and analysis of the 101-story SWFC and the design of 121-story SCT. Subsequently, Tang and Zhao (2014) used the theory of the compensated pile foundation to re-analyze the fully compensated pile-supported raft foundation of the 121-story SCT. Using first-hand data, including a large amount of deformation data, the distinct characteristics of circular structures with diameters of 100 and 123 m and embedments of 18.45 and 31.2 m of the main buildings and embedments of 14 m and 27.6 m of the podiums can be obtained. Such characteristics of two super-tall buildings are uncommon in the world. These problems have to be point out and be discussed in theory and construction.

2. Design theory of TDM

2.1 Construction Process and Loading Characteristics

The TDM remains an advanced technique in excavation engineering. Using this method, the above-ground and underground structures are constructed simultaneously. The key aspect of the TDM is controlling the differential deformation of engineering elements in soft soil. Thus, it is necessary to use soil-structure interaction theory to analyze and minimize the differential deformation between the diaphragm wall and soldier piles and between the central soldier piles such that they do not exceed allowable values. In Shanghai, this value is 20 mm or L/200 (Ministry of construction of P.R. of China, 2002), where L is distance between two adjacent middle soldier piles in mm.

The measured settlements of three skyscrapers in Shanghai, the 88-story Jinmao Building, 101-story Shanghai World Financial Center (SWFC) and 121-story Shanghai Center Tower (SCT), have been proved that piled raft foundation with the thickness of 4.0 m to 6.0 m is still an elastic body. Thus the elastic theory is used in dealing with the superstructure-foundation interaction. We assume that:

(1) The stratum is considered as layered and anisotropic body. The modulus of each layer keeps constant.
(2) The slides between soil and pile are omitted.
(3) The vertical displacements between pile-soil, pile-pile and soil-soil are continuous.

2.2 Interaction of the Pile-supported Raft Foundation During TDM Construction

The theory of interaction between the superstructure and the foundation (Zhao, 1998), including that of pile foundations, is used both in BUM construction and in TDM construction.

(1) The general equation of superstructure-foundation interactions is:

$$([K_b]+[K_r]+[K_{ps}])\{U_b\} = \{S_b\}+\{P_r\} \quad (1)$$

where $[K_b]$ = The condensed equivalent stiffness matrix at the boundary between superstructure and foundation,
$[K_r]$ = The corresponding equivalent stiffness matrix of the bottom slab (raft),
$[K_{ps}]$ = The corresponding equivalent stiffness matrix of the pile-soil interaction system,
$\{U_b\}$ = The corresponding boundary displacement vector,
$\{S_b\}$ = The corresponding boundary load vector condensed to the boundary of the foundation,
$\{P_r\}$ = The corresponding load vector.

(2) Generally, a diaphragm wall with reinforced concrete bracing is used as a retaining wall with a thickness between 800 mm and 1200 mm. It should be noted that the diaphragm wall not only acts as the retaining wall and the outside wall of the basement but can also serve as the bearing structure. In that case, the superstructure, the foundation and the diaphragm wall can be regarded as an integral body. Eq. (1) can be rewritten as:

$$([K_b]+[K_r]+[K_{pws}])\{U_b\} = \{S\}+\{P'_r\} \quad (2)$$

where $[K_r]$ = The corresponding equivalent stiffness matrix of the bottom slab,
$[K_{pws}]$ = The corresponding equivalent stiffness matrix of thepile-soil-wall interaction system, and
$\{U_b\}$ = The corresponding boundary displacement vector,
$\{S_b\}$ = The corresponding boundary load vector condensed,
$\{P'_r\}$ = The corresponding load vector.

$[K_{pws}]$ mobilizes the role of load sharing of the superstructure in practice. Is is calculated from the deformation analysis of a single pile, the interaction analysis between piles, and the analysis of deformation of a unit diaphragm wall, between diaphragm walls, between the diaphragm wall and the pile, between the pile and the diaphragm wall, between the diaphragm wall and the soil, and between the soils. Let N = the nodal number of the pile-soil-wall interaction system, in which m, s and n are the nodal numbers of the pile top, the wall top and the supporting soil, respectively; then $N = m + s + n$, The order vector is the nodal vertical displacement vector of the pile-soil-wall interaction system is:

$$\{w\} = [w_1 \ldots w_m \ \ w_{m+1} \ldots w_{m+1} \ \ \ldots w_{m+s+n}]^T \quad (3)$$

The corresponding nodal reaction force vector of the pile-soil-wall interaction system is given by

$$\{R\} = [R_1 \ldots R_m \ \ R_{m+1} \ldots R_{m+s} \ldots R_{m+s+n}]^T \quad (4)$$

The characteristic function of the pile-soil-wall interaction system is:

$$\{w\} = [\delta]\{R\} \quad (5)$$

in which $[\delta]$ = The flexibility matrix of the pile-soil-wall interaction system and can be expressed as the block matrix

$$[\delta] = \begin{bmatrix} \delta_{pp,ij} & \delta_{pw,ij} & \delta_{ps,ij} \\ \delta_{wp,ij} & \delta_{ww,ij} & \delta_{ws,ij} \\ \delta_{sp,ij} & \delta_{sw,ij} & \delta_{ss,ij} \end{bmatrix} \quad (6)$$

$[K_{pws}] = [\delta]^{-1}$ therefore, Eq. (5) can be rewritten as

$$[K_{pws}]\{w\} = \{R\} \quad (7)$$

in which the vertical displacement vector, $\{w\}$, is also the equivalent boundary displacement vector, $\{U_b\}$.

Equation (2) is the basic equation of the superstructure-foundation-diaphragm wall interactions.

(3) For full TDM construction, we shall analyze the critical condition. When the entire soil mass in the excavation has been removed, the superstructure and the basement have been constructed to i and j stories, respectively, whereas the excavation floor slab has not yet been completed. At this time, the maximum differential settlement will occur. Considering that it will take a certain amount of time for the stiffness of i stories of the superstructure to develop, the stiffness of i-1 stories is only considered, whereas the load of i stories must be considered. Similarly, for the basement, the stiffness of j-1 stories and the load of j stories are considered for safety.

During the critical condition, the raft has not yet poured. According to the theory of interaction between the superstructure and the foundation, when the stiffness of the floor slab $[K_r] \rightarrow 0$, Eq. (2) becomes:

$$([K_{b(j+i-2)}]+[K_{pw}])\{U_b\} = \{S_{j+i}\}+\{P'_r\} \quad (8)$$

where

$[K_{b(j+i-2)}]$ = The condensed equivalent stiffness matrix at the boundary of an i-1-story superstructure and j-1-story basement structure,
$[K_{pw}]$ = The corresponding equivalent stiffness matrix of the soldier pile and the diaphragm wall under the bottom slab,
$\{U_b\}$ = The corresponding boundary displacement vector,
$\{S_{j+i}\}$ = The corresponding boundary load vector condensed to the boundary of the foundation, and
$\{P'_r\}$ = The corresponding load vector of the middle soldier pile and diaphragm wall.

(4) For half-TDM construction, at which time the superstructure has not yet been constructed, Eq. (8) will become:

$$([K_{b(j-1)}]+[K_{pw}])\{U_b\} = \{S_l\}+\{P'_r\} \quad (9)$$

Using Eq. (8), the corresponding program can be formulated. A flowchart of the program for TDM construction is shown in Fig. 1.

The elastic theory can be used to calculate the pile raft foundation.

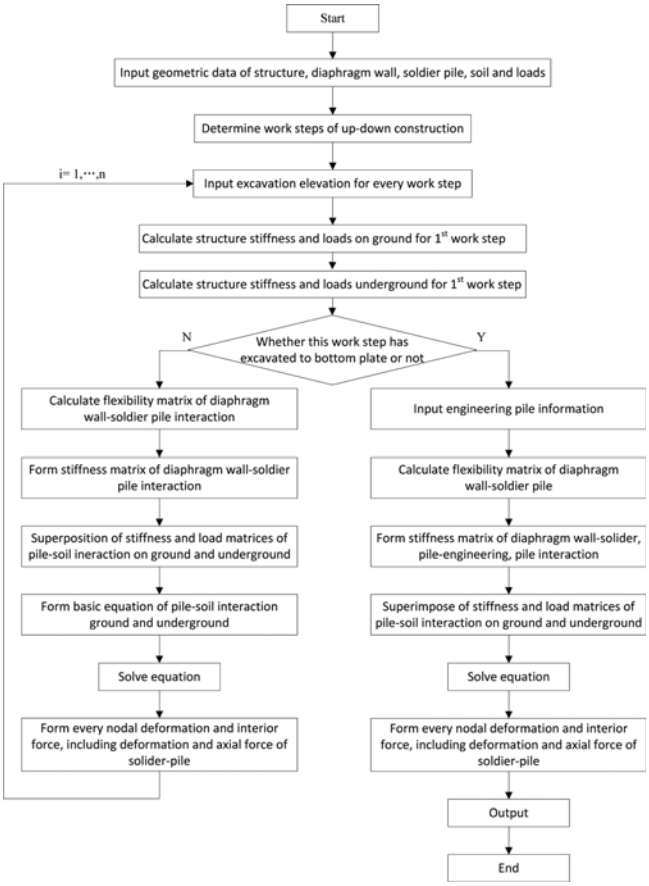

Fig. 1. Flow Chart of Analysis of TDM Construction

The soil behavior is nonlinear indeed. However, for piled raft foundation with deep embedment and long pile of tall and super-tall buildings, the shape of settlement is almost a pot and load distribution on the top of pile group for equal length of pile and basic rectangular plane of foundation is regular on an elastic foundation. In that case, the soil behavior is assumed to be elastic in practice.

Based on the analysis of results of pile loading tests for the single pile and engineering experience, we found an approximate relationship between the value of E_0 and the weighted average value of compressibility modulus, $E_{S0.1\text{-}0.2}$ within the range of the pile length $E_0 = 3E_{S0.1\text{-}0.2}$. So, the value of E_0 in this paper is taken as $3E_{S0.1\text{-}0.2}$ when employing superstructure-foundation interaction method.

3. CFM Building

The CFM was built using half TDM construction. This 60-story (238-m tall) building is founded on a 4.5 to 6.25 m thick raft and cast in a cast-in-situ piles, including soldier piles, 850 mm in diameter driven into a silty, medium to coarse sand layer (the ⑨$_2$ soil layer, Table 1). These piles were cast in drilled shafts to a depth of 72.5 m at a center-to-center horizontal spacing of 2.66 m. A 10-story podium is supported by a 2-m-thick raft and cast in drilled shaft piles that are of the same dimensions and layout as the piles of the main building. Both the main building and podium have 4-story basements. The outer wall of the basement consists of the diaphragm wall, which is 800 mm to 1000 mm thick. This wall's depth of embedment is approximately 18.95 m (podium) to 24.7 m (main building) below the ground surface. The total area of the foundation pit is approximately 25,890 m^2 and is divided into 4 zones for construction. The site plan and the instrument layout are shown in Fig. 2. Table 1 lists the important physical and mechanical properties of the soil layers. The concrete grade of diaphragm walls and soldier piles is C40. The average groundwater level is approximately 0.5 m

Table 1. Physical and Mechanical Properties of Soil at the CFM Site

Soil layerno.	Soil description*	Depth (m)	$Es_{0.1\text{-}0.2}$ (Mpa)	W (%)	γ (kN/m^3)	e_0	c_{cu} (kPa)	ϕ_{cu} (°)	c' (kPa)	ϕ' (°)
①	Fill	1.8								
②	Clay	2.5	4.60	32.9	18.3	0.94	16	21.8	1	32.5
③	Very soft silty clay	7.1	3.52	41.4	17.4	1.17	11	23.2	0	34.0
④	Very soft clay	15.0	2.21	50.8	16.6	1.43	10	14.0	2	29.5
⑤$_{1\text{-}1}$	Clay	22.3	3.69	39.2	17.5	1.14	17	16.7	1	29.7
⑤$_{1\text{-}2}$	Silty clay	28.0	4.75	34.9	17.8	1.02	21	23.7	0	31.0
⑤$_{3\text{-}1}$	Silty clay with M.S.	42.0	5.39	34.1	17.9	1.00	13	29.4	0	35.5
⑦$_2$	Silty fine sand	44.7	15.81	26.3	19.1	0.74				
⑧$_1$	Clay	52.3	6.02	35.4	18.0	1.02				
⑧$_2$	Silty clay with S.M.	58.0	5.19	32.5	18.2	0.94				
⑨$_{1\text{-}1}$	Silty fine sand	67.3	15.29	26.7	19.0	0.76				
⑨$_{1\text{-}2}$	Silty clay	70.4	8.33	23.8	20.0	0.65				
⑨$_{1\text{-}3}$	Silty fine sand	76.5								
⑨	Medium sand with G.	92.5	21.10	20.1	19.8	0.60				
⑩	Silty clay	97.5	12.92	25.7	19.1	0.74				
⑪	Fine sand	106.4	14.99	26.3	19.4	0.74				

Note: M.S. denotes clayey silt, S.M. denotes silty sand, and G. denotes gravel. $Es_{0.1\text{-}0.2}$ denotes compressive modulus under the compressive pressure of 0.1-02 MPa.

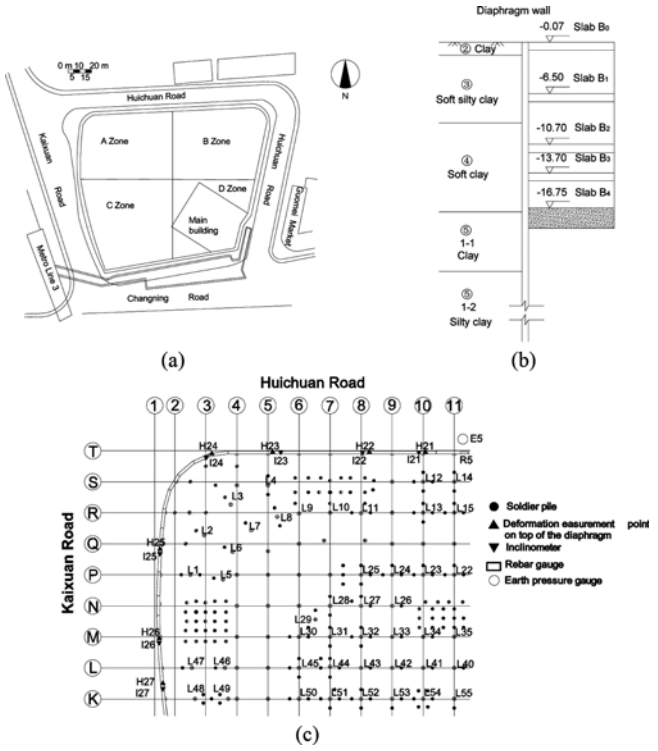

Fig. 2. Site Plan, Section Through Bracing System, and Layout of Bracing System and Instruments: (a) Site Plan, (b) Section Through Bracing System in Zone A, (c) Layout of Bracing System and Instruments in Zone A

Table 2. Excavation Sequence for CFM Project

Stage	Date	Construction activity
1a	August 6, 2003	Excavation to depth of 0.27 m
1	September 10, 2003	Slab B0 (top slab of the first basement) complete
2a	October 17, 2003	Excavation to depth of 6.7 m
2	November 9, 2003	Slab B1 (top slab of the second basement) complete
3a	November 27, 2003	Excavation to depth of 11.6 m
3	December 28, 2003	Slab B2 (top slab of the third basement) complete
4a	April 11, 2004	Excavation to depth of 14.6 m
4	May 5, 2004	Slab B3 (top slab of the fourth basement) complete
5a	June 10, 2004	Excavation to depth of 18.95 m
5	July 7, 2004	Raft, slab B4 (bottom slab of the fourth basement)
6	July 31, 2004	Raft or B4 consolidate

below the ground surface. The excavation sequence of this CFM case history is presented in Table 2.

3.1 Computation and Field Test of CFM

There are 4 basement levels. The slabs (B0, B1, B2, B3 and B4 or raft) are 200, 150, 200 and 2000 mm thick, respectively, and the combined dead and construction loads on each slab is 0.75 kN/m^2. Based on the 2-D top-down construction theory along grid line L, as shown in Fig. 2(c), the deformation of the diaphragm wall, the soil behind the wall and the soldier piles are computed, as are the axial forces on the wall and soldier piles, the bending moment in the slab and the stress in the wall at construction stages 1-6.

The computed deformation, including the heave, settlement and lateral wall deflection, the axial force on the diaphragm wall and soldier piles and the maximum moment in the slab along grid line L in Zone A were analyzed at various stages during the entire TDM construction sequence. Afterward, the corresponding measured data were analyzed.

3.1.1 Computed Deformation and Internal Forces in the Diaphragm and Soldier Piles

Owing to space limitations, only the computed results corresponding to construction stages 5 and 6 (Fig. 3), are presented.

The maximum deformations, axial forces and moments at five construction stages are summarized. The maximum deformation of and axial force on the diaphragm wall and soldier piles and maximum moment in the slab are listed in Table 3.

3.1.2 Computed Deformations of the Diaphragm Wall and Soldier Piles

The deformations of the diaphragm wall and soldier piles at various construction stages along grid line L in Zone A are listed Table 4. Point 1 represents the position of the diaphragm wall on grid line L. Points 2 through 11 represent the positions of soldier piles at the intersections of grid lines 2 through 11, respectively, on grid line L.

The computed deformations increase as the construction progresses (Table 4). Before the placement of the raft, i.e., at stage 5, the maximum deformation was 23.25 mm, at grid line 8. Afterward, the maximum deformation was 36.96 mm.

The heave at stage 6 reflects the fact that the concrete has been poured. At that time, the basement, the diaphragm wall, the soldier piles, the raft and the engineered pile rafts are connected and form an integrated unit. Based on the results from stage 6, the load sharing of the diaphragm (loading) wall can be computed as described in Section 3.4.

The computed differential deformations between the wall and soldier pile 2 increase through stages 2 to 6, with values of 3.22 mm, 5.86 mm, 8.14 mm, 10.13 mm and 4.68 mm, respectively. As mentioned above, these deformations are due to the interactions following the completion of construction.

After the raft placement, the shape of the deformation changes to that of an arc as expected.

3.1.3 Computed Axial Forces on Diaphragm Wall and Piles

Based on the axial forces during construction stages 5 and 6, a summary of the axial forces is shown in Fig. 3.

When the maximum moment in the raft is 3301 kN-m/m (Table 3) and the corresponding maximum rebar tensile stress is only 1,238 kPa/m, based on the plane section assumption (Park and Pauley 1975), which is much less than the allowable stress. This

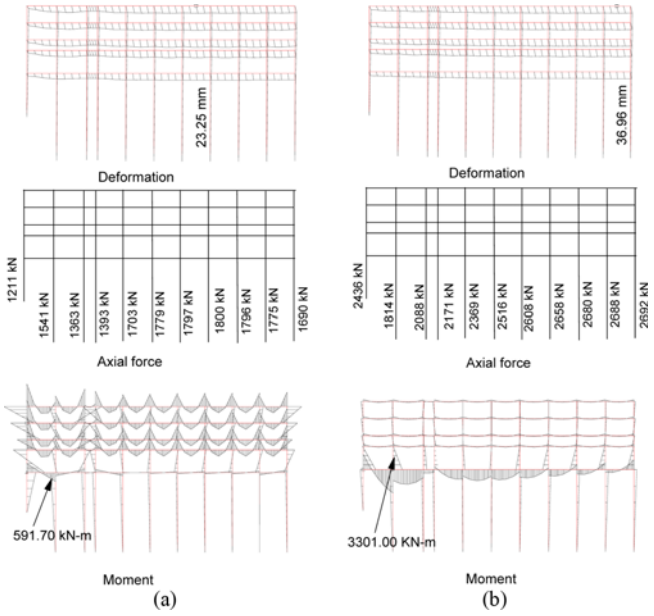

Fig. 3. Distribution of Deformations, Axial Forces and Moments: (a) Construction Stage 5, (b) Construction Stage 6

Table 3. Maximum Deformations, Axial Forces and Moments

Construction stage	Max. deformation (mm)	Max. axial force (kN)	Max. moment (kN-m)
Stage 2	5.61	452.20	418.40
Stage 3	11.35	901.40	487.60
Stage 4	17.23	1351.00	543.10
Stage 5	23.25	1800.00	591.70
Stage 6	36.96	2692.00	3301.00

redistribution is the most distinct characteristic of the TDM construction.

3.1.4 Measured Deformations (vertical displacements) of the Diaphragm Wall and Piles

The measurement period began on Oct. 14, 2003, and ended on July 31, 2004. Before the raft placement, measurements were collected on the piles (stage 5) and diaphragm wall on July 4 and 6, 2004, respectively. After the raft placement, measurements were collected on the piles and wall on July 11 and 16, 2004, respectively.

The excavation began on Aug. 6, 2003. Before the raft placement, the maximum heave of diaphragm wall point H24 was 11.1 mm, whereas after the raft placement, the maximum settlement of the same point was 3.7 mm. After the raft placement, the entire diaphragm wall caused settlement due to the loading and consolidation from the concrete.

Due to the heave of all 55 soldier piles, the general data from only the most noteworthy stage of construction are presented; data are presented in detail in Sections 3.1.5 and 3.1.6.

Before and after placement of the raft (slab B4), the maximum amounts of heave among all soldier piles L1-L55 are 6.2 mm and 5.8 mm.

3.1.5 Measured Differential Deformations

The measured differential deformations (vertical displacements) between the diaphragm wall and soldier piles and between the piles are listed in Table 5.

The differential deformations (vertical displacements) immediately before and after raft placement (stages 5a and 5).

(1) The differential deformations between the piles are 3.7 mm and 4.1 mm before and after raft placement, respectively.
(2) The differential deformations between the wall and soldier pile L47 are 17.0 mm and 15.9 mm, respectively.
(3) The differential deformations between wall point H23 and soldier pile L4 are 8.2 mm and 6.3 mm, respectively.

To proceed further with the analysis, the computed deformations, axial forces and moments along grid line L in Zone A, are compared with the corresponding measured deformation. Table 6 lists the measured deformations of diaphragm wall H and piles L47, L46, L45, L44, L43, L42, L41 and L40.

The differential deformations between the soldier piles are small, whereas the differential deformation between the wall and soldier pile L47 is large. Before the raft placement, the maximum wall-to-pile differential deformation (July 4-6, 2004) was 17.0 mm. After the raft placement, this amount was 15.9 mm less than

Table 4. Deformation of Diaphragm Wall and Soldier Piles at Various Construction Stages Along Grid Line L in Zone A (mm)

Point No.	1	2	3	4	5	6	7	8	9	10	11
Stage 2	2.08	5.30	4.12	4.21	5.43	5.59	5.61	5.61	5.60	5.55	5.12
Stage 3	4.44	10.30	8.45	8.64	10.88	11.27	11.34	11.35	11.33	11.20	10.48
Stage 4	7.00	15.14	12.95	13.24	16.40	17.07	17.21	17.23	17.19	17.00	16.06
Stage 5	9.77	19.90	17.61	17.99	21.99	22.97	23.21	23.25	23.20	22.93	21.83
Stage 6	20.56	25.24	28.88	29.98	32.63	34.59	35.83	36.50	36.80	36.90	36.96

Note: Point 1 represents the diaphragm wall midway between measurement points H26 and H27.

Table 5. Maximum Measured Differential Deformation (mm)

Stage No.	1a	1	2a	2	3a	3	4a	4	5a	5
Max. value between soldier piles	3.5	3.4	3.0	2.2	2.1	2.1	2.7	2.6	3.7	4.1
Value between wall H and soldier pile L47	4.8	8.7	9.4	9.5	8.6	8.6	11.0	10.0	17.0	15.9
Value between wall point H23 and soldier pile L4	7.5	3.4	6.9	8.0	7.0	5.7	9.3	7.3	8.2	6.3

Note: Deformation of wall H is taken as the average deformation at points H26 and H27.

Table 6. Measured Deformations Along Grid line L in Zone A (mm)

Measured point	H	L47	L46	L45	L44	L43	L42	L41	L40
Stage 2a	-7.8	1.4	0.8	2.2	2.5	2.5	3.5	3.4	2.5
Stage 3a	-7.6	3.7	1.9	3.7	3.6	2.7	4.7	2.5	3.1
Stage 4a	-5.2	2.1	2.1	3.3	3.9	2.3	4.4	2.9	3.9
Stage 4	-3.5	4.4	3.6	2.4	3.1	1.9	4.5	2.7	2.5
Stage 5a	-11.2	5.8	5.0	3.2	4.4	0.7	4.0	1.9	1.6
Stage 5	-11.5	4.4	3.2	3.6	4.4	0.3	2.5	1.8	1.6

Note: Deformation of wall H is taken as the average of the deformation at points H26 and H27 (Fig. 3c).

Table 7. The Maximum Computed and Measured Deformation and Differential Deformation (mm)

Position	H		L41		H & L46		L46 and L47	
	Computed	Measured	Computed	Measured	Computed	Measured	Computed	Measured
Stage 5	9.77	11.2	22.93	1.9	10.13	17.0	2.29	0.8
Stage 6	20.56	11.5	36.90	1.8	4.68	15.9	3.64	1.2

the allowable value, 20 mm. These valuable data emphasize the importance of the differential deformation between the diaphragm wall and the nearest soldier pile.

3.1.6 Comparison between Computed and Measured Deformations and Differential Deformations

The computed and measured maximum deformations and differential deformations before and after the raft placement were obtained from Tables 5-6 and listed in Table 7 for comparison between the computed and measured values.

Judging from the results shown in Table 7, the computed results are satisfactory, although the computed and measured post-concrete placement values differ significantly, as discussed in Section 6.

After the raft placement, the profile of the settlement is an arc. The deformation of the diaphragm wall increased from 9.77 mm to 20.56 mm, and the differential deformation decreased from 10.13 mm to 4.68 mm, which was due to the interaction of the entire structure and the loading and consolidation by the raft.

3.2 Earth Pressures (lateral pressures) on Diaphragm Wall

Earth pressure cells were placed along the wall at depths of 5 m, 10 m, 15 m, 20 m and 25 m to measure the earth pressures on the retaining wall. The measured and computed results (Fig. 4) shows that the measured earth pressure-depth curve is essentially a straight line, whereas the other three curves (three computational methods) display values that exceed the measured values by approximately 50~100%. The calculated earth pressures based on the effective stress and total stress decrease slightly with depth, whereas the calculated at-rest earth pressures plot essentially on a straight line near those calculated using the effective-stress method.

3.3 Stress in Diaphragm Wall

The stress in the diaphragm wall is related to the loading on the wall. However, the many measurements demonstrate that the measured stress in the wall is less than the allowable steel stress. Three sets of rebar stress gauges, designated R5, were placed along the wall at depths of 5 m, 10 m, 15 m, 20 m and 25 m to measure the stress on the steel in the retaining wall. The measured results (Fig. 5) shows that the steel stresses in the diaphragm wall decrease with depth. The maximum steel stress is 1.3 MPa, which is 1/10 of the predicted stress. Therefore, the design may be considered conservative.

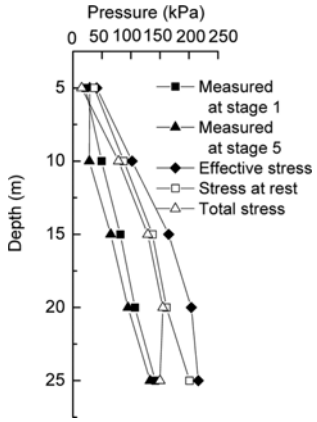

Fig. 4. Curves of Earth Pressure vs. Depth at the CFM Site

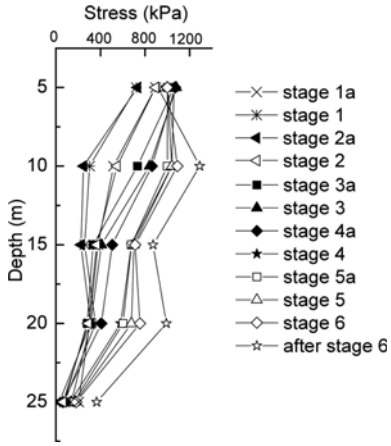

Fig. 5. Stress-depth-time Curve at Point R5 in the Diaphragm Wall

3.4 Load Sharing by Diaphragm Wall

In Zone A, the length of the periphery of the diaphragm wall is approximately 152 m, and the total number of soldier piles is 55. Before the raft placement, stage 5 is the most noteworthy construction stage. The axial forces on the diaphragm wall and on the soldier piles after the placement of the raft are shown in Fig. 3(b). The computed load sharing by the diaphragm wall is 9.8% of the combined structural and construction loads, which demonstrates one of the advantages of TDM construction.

3.5 De-watering of Confined Water

De-watering is one of key factors affecting the structural safety during top-down construction. The initial water level is 0.5 m below the ground surface. In this case, the depth of excavation was 22 m below the main building and 18.95 m below the podium. To prevent soil heave and associated effects on adjacent properties due to rising water pressure, it was necessary to perform de-watering of the confined water level.

4. LCXFC Building

The 37-story LCXFC building is 170 m tall including the 3-story podium. Both structures have a 5-level basement. The average depth of excavation was 22.4 m (podium) and 28.4 m (main building). The total area of the foundation pit was approximately 25,890 m^2. The structures are supported on a raft-pile foundation. The rafts for the main building and podium are 3.00 m and 2.00 m thick, respectively. The piles are cast in drilled shaft piles with 850 mm and 1100 mm diameters. The piles total 460 and are 71 m long; there are only 126 soldier piles (850 mm diameter). The diaphragm wall is 1000 mm thick and 35 m long.

The environment around this building is comparatively complex, as shown in Fig. 6(a). In this building, considering that the height from the last slab to the bottom of the foundation pit is 7.4 m, safety required the installation of a temporary concrete brace to reinforce the structural stiffness (Fig. 7(b)), the site plan and the instrument layout are shown in Fig. 7(c). The selected physical-mechanical properties of the soil layers are presented in Table 8. The concrete grade of diaphragm walls and soldier piles is C40. The average groundwater level is approximately 0.8 m below the ground surface. The excavation sequence is presented in Table 9.

4.1 Computations and Field Testing at LCXFC Site

There are 5 basement levels. The slabs (B0, B1, B2, B3, B4, and B5 or raft) are 200 mm, 150 mm, 150 mm, 200 mm, 200 mm and 3,000 mm thick, and the total dead and construction load on the slab is 0.75 kN/m^2. Based on the 2-D TDM construction theory, the deformation of the diaphragm wall, the soil behind the wall and the soldier piles are computed, as are the axial forces on the wall and the soldier piles and the moments in the slab and the stress in the wall along grid line D at construction stages 1-6. Due to space limitations, the results corresponding to stages 3 through 6 are listed in Table 10.

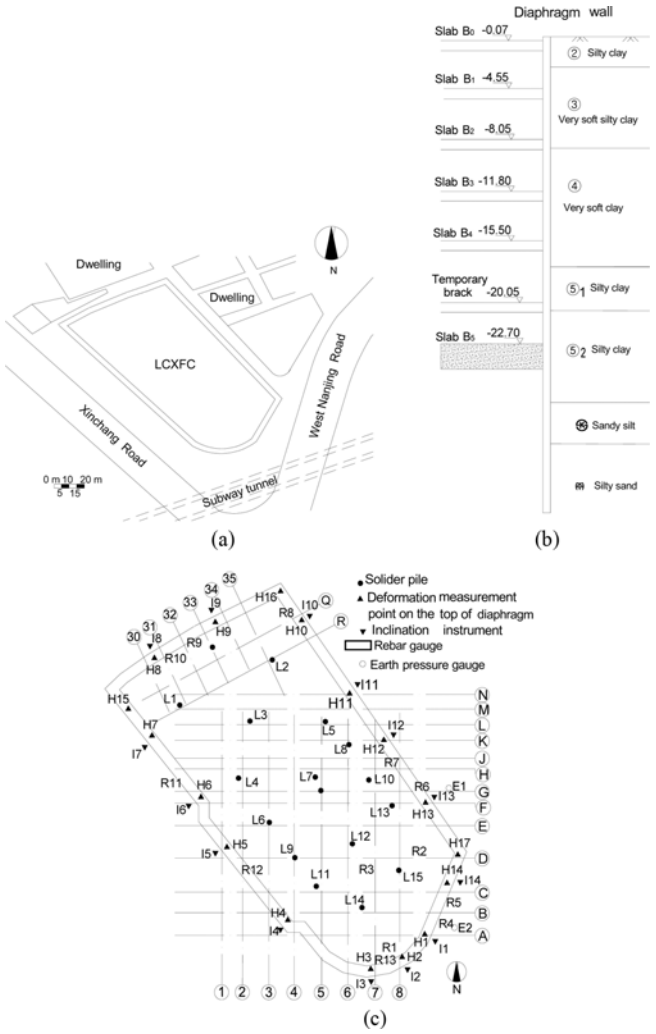

Fig. 6. Site Plan, Section Through the Bracing System, and Layout of the Instruments: (a) Site Plan of the LCXFC Building, (b) Section Through the Bracing System of the Diaphragm Wall, (c) Layout of the Instruments

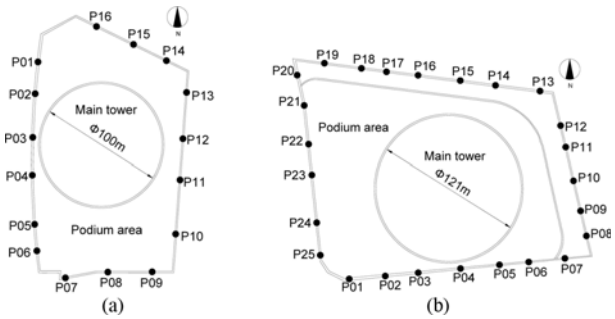

Fig. 7. Site Plans and Locations of Inclinometers: (a) SWFC, (b) SCT

4.1.1 Computed Deformation of Diaphragm Wall and Soldier Piles

The computed deformations of the diaphragm wall and the soldier piles at 4 construction stages along grid line D are presented in Table 11. Point 1 represents the position of the diaphragm wall

Table 8. Physical and Mechanical Properties of Soil at the LCXFC Site

Soil layer no.	Soil description	Depth m	γ (kN/m^3)	Cohesion (kPa)	ϕ' (°)	Modulus of compression (MPa)	Permeability coefficient	
							k_H (10^{-7} cm/s)	k_V (10^{-7} cm/s)
①	Fill	1.5	--	--	--	--	--	--
②	Brown-yellow silty clay	1.6	18.9	17.0	20.0	5.11	2.15	1.42
③	Grey, very soft, silty clay	5.3	17.8	13.0	20.0	4.08	100	1.63
④	Grey, very soft clay	8.7	17.1	13.0	10.5	2.45	1.4	0.8
⑤$_1$	Grey clay	3.0	17.8	16.0	11.5	4.88	147	1.15
⑤$_2$	Grey silty clay	6.8	18.2	13.0	21.2	8.00	2.56	1.88
⑥	Dark green silty clay	3.0	20.1	42.80	21.4	9.15	45	--
⑦$_1$	Grass-yellow sandy silty	8.5	18.8	5.71	39.14	12.38	240	--
⑦$_2$	Yellow silty sand	10.5	19.0	4.29	41.79	14.35	1100	--
⑦$_3$	Grey silty sand	4.5	19.1	5.71	41.43	15.43	11,000	--

Table 9. Excavation Sequence of LCXFC Project

Stage	Date	Construction activity
1a	January 3, 2004	Excavation to -2.55 m
1b	Febuary. 10, 2004	Slab B0 complete at elevation -0.5 m
1c	March 15, 2004	Excavation to -6.40 m
1	April 20, 2004	Slab B1 complete at elevation -4.55 m
2a	May 27, 2004	Excavation to -9.90 m
2	June 21, 2004	Slab B2 complete at elevation -8.05 m
3a	August 5, 2004	Excavation to -13.70 m
3	September 5, 2004	Slab B3 complete at elevation -11.8 m
4a	September 16, 2004	Excavation to -17.2 m
4	October 18, 2004	Slab B4 complete at elevation -15.5 m
5a	November 20, 2004	Excavation to -20.4 m
5	December 26, 2004	Temporary strut at elevation -20.05 m
6a	January 5, 2005	Excavation to -22.7 m
6	Febuary 4, 2005	Raft complete

Table 10. Maximum Deformations of and Axial Forces on Diaphragm Wall and Soldier Piles and Maximum Moments in the Slab

Construction stage*	Max. deformation (mm)	Max. axial force (kN)	Max. moment (kN-m)
Stage 3	3.0	1017	368
Stage 4	9.0	1820	480
Stage 5	13.3	1906	466
Stage 6	29.0	2539	476

*Note: Stages 1 and 2 are omitted due to their small deformation values.

along grid line D. Points 2 through 8 indicate the positions of soldier piles at the intersections of grid lines 2 through 8, respectively, and grid line L.

The deformations of the diaphragm wall and the soldier piles all consist of heave during the entire excavation process. The maximum heave at stage 6 is 29 mm.

4.1.2 Computed Axial Forces on Diaphragm Wall and Soldier Piles

The computed axial forces on the diaphragm wall and the soldier piles at the 4 construction stages are summarized in Table 12. That the maximum axial force on soldier pile 4 is 2539 kN, at stage 6, corresponding to the maximum heave of 29.0 mm at the same stage, as shown in Table 11. It was predicted that after the raft placement, the stiffness of the complete structure would change to that of a structural unit, and the load on the engineering piles would also be redistributed.

Table 11. Computed Deformations (heave) of Diaphragm Wall and Soldier Piles at 4 Construction Stages (mm)

Point No.	1	2	3	4	5	6	7	8
Stage 3	1.5	1.7	2.0	3.0	2.0	1.8	2.0	1.8
Stage 4	5.9	6.5	7.1	9.0	7.1	6.8	7.2	6.5
Stage 5	9.3	11.4	12.2	13.3	12.2	11.6	10.3	9.7
Stage 6	25.1	26.7	27.5	29.0	27.5	26.6	25.2	25.2

4.1.3 Measured Deformations of Diaphragm Wall

Due to the TDM construction, the horizontal displacement is very small and thus can be ignored. Only the vertical deformations (heave) are listed in Table 13. Measurement points H1 through H17 were established along the diaphragm wall along the periphery of the excavation (Fig. 6(c)). The deformations during the entire excavation sequence and the deformations of the diaphragm wall (Table 13) consisted of heave and are the same as the computed deformations, as discussed in Section 4.1.1. The measured heave at stage 4 varies from 6.1 mm to 15.4 mm.

4.1.4 Measured Deformations of Soldier Piles

Measurement points L1 through L15 were distributed throughout the excavation for measuring the deformation of the soldier piles (Fig. 6(c)). The middle column grid is basically 8.4 m × 7.0 m throughout the excavation sequence, and the deformations of the soldier piles all increased as the construction progressed. At the end of the excavation construction, the deformations were range from 13.9 to 35.9 mm. In contrast, at construction stage 4, the differential deformations between the diaphragm wall and the adjacent soldier pile and between the soldier piles all decreased. The deformations of the soldier piles all consisted of heave throughout the excavation sequence and are the same as the

Table 12. The Computed Axial Forces on the Diaphragm and Soldier Piles (kN)

Point No.	1	2	3	4	5	6	7	8
Stage 3	577	916	791	1017	790	881	799	278
Stage 4	754	1299	1018	1693	1020	1168	1454	304
Stage 5	848	1867	1481	1906	1477	1746	1398	359
Stage 6	912	2251	1918	2539	1916	2271	1471	419

Note: Point No. 1 represents Wall 1, and other numbers represent soldier piles 2-8.

Table 13. Measured Deformation (heave) of Diaphragm Wall and Piles at Stage 4 (mm)

Point No.	Heave	Point No.	Heave	Point No.	Heave	Point No.	Heave	Point No.	Heave
H1	13.7	H8	6.1	H15	12.6	L5	17.4	L12	27.0
H2	12.9	H9	8.1	H16	15.4	L6	19.3	L13	24.9
H3	9.5	H10	9.1	H17	14.7	L7	20.7	L14	29.0
H4	9.5	H11	12.7	L1	13.9	L8	22.1	L15	21.9
H5	14.6	H12	14.8	L2	14.5	L9	26.08		
H6	11.5	H13	14.1	L3	21.8	L10	17.6		
H7	10.0	H14	14.0	L4	19.2	L11	19.3		

Table 14. Computed and Measured Deformation Along Grid Line D at Stage 4 (mm)

Point No.	1	2	3	4	5	6	7	8
Computed	25.1	26.7	27.5	29.0	27.5	26.6	25.2	25.2
Measured	14.6 (H5)		26.08 (L9)		27.00 (L12)		21.90 (L15)	

Note: Point No. 1 represents Wall 1, and the other points represent soldier piles 2-8.

computed deformations.

4.1.5 Comparison of Computed and Measured Deformations (vertical displacements)

The computed and the measured deformations of the diaphragm wall and the soldier piles along grid line D at stage 4 were compared. The computed values were taken from stage 4 in Table 11, and the measured values at point H5 and points L9, L12 and L15 from Table 13, which are near the computed points, were used. The results of the comparison are presented in Table 14. The computed and measured deformations of the diaphragm wall and the soldier piles are approximately equal, with the exception of the values on the wall. The reason for this difference is discussed in Section 6.

4.1.6 Measured Deflections of Diaphragm Wall

The measured deflections of the diaphragm wall at measurement points I1 through I14 are presented in Table 15. The maximum deflections are between 20.01 mm and 34.59 mm.

When the maximum deflection at I10 is taken as 34.59 mm and the embedment, D, is taken as 22.4 m, then the ratio of deflection, S_h to D, is 0.0015:

$$S_h \approx 0.15\%\ D \tag{10}$$

However, the statistical-empirical formula $S_h \approx 0.15\%$ D is used to predict the deflection for the BUM and not for the TDM. Thus, this calculated value is more than the value usually used in practice, which could be due to certain aspects of the construction.

Table 15. Deflection of Diaphragm Wall at Points I1 Through I14 (mm)

Point No.	Max. displacement	Point No.	Max. displacement	Point No.	Max. displacement
I1	31.01	I6	27.39	I11	25.86
I2	21.64	I7	28.74	I12	33.63
I3	21.36	I8	26.92	I13	20.01
I4	23.76	I9	29.42	I14	26.36
I5	23.83	I10	34.59		

Table 16. Maximum Shear and Moment Forces in the Slab at 4 Construction Stages

Stage No.	Maximum shear (kN)	Maximum moment (kN-m)
Stage 2	230	368
Stage 3	288	498
Stage 4	240	466
Stage 5	278	476

4.1.7 Measured Brace Axial Force, Slab Stress, and Shear and Moment Forces in the Slab

In this Section, the measured brace axial force and the slab stress are briefly discussed. During the entire sequence of construction, the maximum brace axial force was 392 kN, whereas the maximum stress in the slabs was 5,414 kPa.

The maximum shear and moment forces in the slab at 4 construction stages are presented in Table 16. The shear and moment forces appear to either increase or decrease slightly as the construction progresses and the structural stiffness increases.

Therefore, the brace axial forces, slab stresses, and shear stresses are less than the allowable values.

4.2 Load Sharing by the Diaphragm Wall

Based on the computed axial forces on the diaphragm wall and the soldier piles (Table 12). Based on these data, the diaphragm wall can share the structural load at various construction stages, as

Table 17. Computed Sharing of Load by Wall

Stage No.	Total load (kN)	Share of load taken by wall (%)
Stage 2	6049	14.1
Stage 3	8710	12.1
Stage 4	11,082	10.9
Stage 5	13,697	9.7

listed in Table 17. The structural stiffness increases as the construction progresses, and the loads on the diaphragm wall decrease from 14.1% at construction stage 2 to 9.7% at construction stage 5. In other words the diaphragm wall can share 9.7% of the structural load.

4.3 De-watering of Confined Water

As in Section 3.5., de-watering is an important factor in the structural safety. Confined water is one of the complex factors in construction.

In this project, confined water is primarily present in layer ⑦ (Table 8), which consists of sandy silt and silty sand, and in layer ⑦, a silty fine sand. The de-watering focused on the confined water in layer ⑦, and it was predicted that water from layer ⑨ may flow into layer ⑦ during de-watering, which is an important effect that should be considered. Layer ⑦ is present at depth of 30.80 m.

The testing of the well-point de-watering plan occurred from Aug. 2, 2004, through Jan. 3, 2005. During the entire excavation sequence, no water problems occurred.

During construction, measurements of earth pressures on and stresses in the diaphragm wall could not be obtained due to the destruction of the earth pressure cells and the rebar during construction.

At the end of the descriptions of the CFM and LCXFC buildings, it should be noted that the authors selected two typical tall buildings. The field testing was first conducted in Shanghai on the CFM, whereas the deepest excavation was created during construction of the LCXFC. Engineering practice has demonstrated that the computed results based on the superstructure-foundation interactions and statistical-empirical formula presented by the authors essentially agreed with the measurements. Throughout the construction process, the differential deformations and lateral wall deflections were controllable using normal practices and did not affect the surrounding environment or the adjacent buildings and structures.

With the rapid development of super-tall buildings in Shanghai, the field testing during construction of the SWFC and the design of the SCT in which the authors participated, provided a rare opportunity to study two buildings with circular excavation structures and deep embedments. The BUM and TDM were used in constructing the main building and the podium, respectively. A comparison of the methods used to construct these buildings and the CFM and LCXFCs' rectangular excavations allows for a very useful analysis of the problems associated with TDM.

5. Excavations for the SWFC and SCT

The SWFC, with an area of 7,855 m^2 in the main building and 14,600 m^2 in the podium, and the SCT, with an area of 11,500 m^2 in the main building and 23,460 m^2 in the podium, required round deep excavations for the main buildings and irregular excavations for the podiums (Fig. 7). The podium excavations are 15 m and 27.6 m deep below the SWFC and SCT, respectively. The main building excavations are 18.45 m and 31.20 m deep below the SWFC and SCT, respectively. Their geotechnical profiles are similar (Tang and Zhao, 2015). The concrete grade of diaphragm walls and soldier piles is C40.

The locations of the inclinometers installed along the diaphragm walls (Fig. 7). The main buildings were built using the BUM, whereas the podiums were built using the TDM.

5.1 Measured Deformation of Excavation Structures

To compare the deflection associated with the TDM construction

Table 18. Heave and Deflection of Main Buildings (mm)

Building	Heave	Deflection
SWFC	27.5	30.0
SCT	68.5	68.5

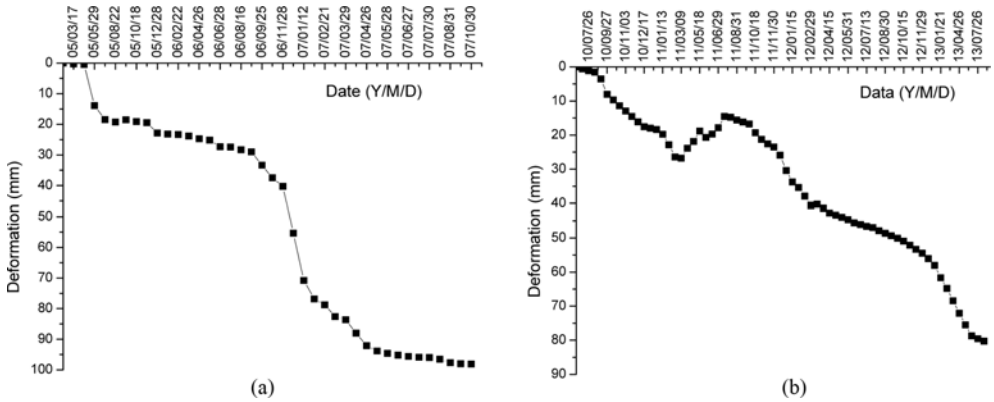

Fig. 8. Deformation vs. Time at the SWFC and SCT Sites: (a) SWFC (Tang and Zhao 2014), (b) SCT

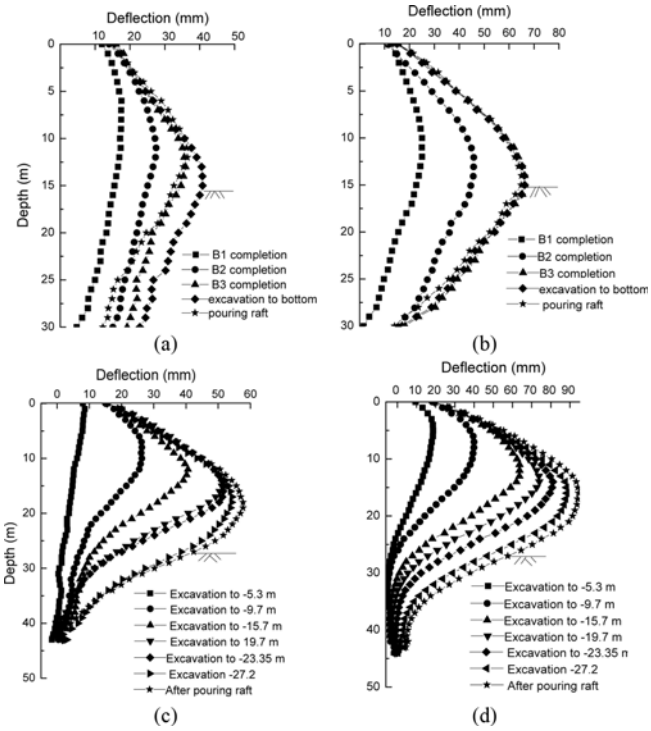

Fig. 9. Deflection of Podium vs. Depth: (a) P03, SWFC, (b) P08, SWFC, (c) P04, SCT, (d) P23, SCT

Table 19. Selected Deflections of Podium (mm)

Depth (m)	P03, SWFC	P04, SCT	P08, SWFC	P23, SCT
15	42.0	57.5	65.6	94.0
27	N/A	47.5	N/A	50.0

Note: Points P03 (SWFC) and P04 (SCT) are approximately 5 m from the main buildings. Points P08 (SWFC) and P23 (SCT) are approximately 51 m from the main buildings.

of the two buildings, we selected the measurement points (Fig. 7) P03 and P08 at the SWFC site and points P04, P23 at the SCT site. The heaves and deflections of the bottom of the raft are presented in Table 18.

There was no measured heave in the SCT buildings. A heave of 68.5 mm was predicted from the deflection of the diaphragm wall of 68.5 mm, and thus the heave was inferred from the curve of deformation vs. time, shown in Fig. 8(b). The deformation was obtained at the point where the construction weight equaled the self-weight of the excavation pit divided by 1.2, i.e., 76.0/1.2 = 63.3 mm. Using this method, the heave in the SWFC can be reduced using Fig. 8(a) if measured data are lacking. The deflections of the podiums at the selected depths are listed in Table 19, and curves of the deflection vs. depth at various construction stages are shown in Fig. 9.

5.2 Deformation Associated with the TDM

5.2.1 Deformation During TDM Construction

Points P23 (SCT) and P08 (SWFC) are located approximately 51 m from their respective diaphragm walls. Point P23 is located

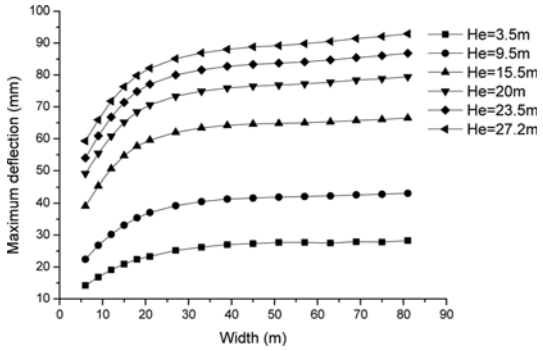

Fig. 10. Width of Excavation vs. Deformation of the SCT Podium

on the west side of the SCT, and point P08 is located on the south side of SWFC. The deflection of the diaphragm wall at P23 is greater than that at P08, i.e., 94.0 mm/65.6 mm = 1.43.

Similarly, the distances of point P04 (south side of the SCT) and point P03 (south side of the SWFC) to their respective diaphragm walls are approximately 5 m. The lateral wall deflection at P04 is greater than that at P03, i.e., 57.5 mm/42.0 mm = 1.37.

Therefore, the lateral wall deflection ratios of the measurement points located similar distances from the SWFC and SCT are 1.43 and 1.37, respectively. The average ratio is 1.40, which can be used for reference in practice.

5.2.2 Deflection vs. Depth

Figures 9(c) and 9(d) show that the excavation for the podium of the SCT is 27.6 m deep, and the maximum lateral wall deflection occurs at a depth of 15-20 m, below which the lateral wall deflection decreases with an increase in depth.

Figures 9(a) and 9(b) show that the excavation for the podium of the SWFC is 15.0 m deep, and the maximum lateral wall deflection occurs at a depth of precisely 15 m, below which the lateral wall deflection decreases with an increase in depth.

5.2.3 Deflections vs. the Width

Based on published data (Mana and Clough 1981) and the computed results (Fig. 10), the relationship between the lateral wall deflection and the width of the pit is very evident and readily understood. From Fig. 10, when the excavation exceeds a width of approximately 35 m, there is little additional effect on the lateral wall deflection.

In this section it should be noted that Fig. 8(b) in SCT shows the deformation-time curve from January 3, 2011 to August 31, 2011 during construction due to ceasing de-watering and the corresponding deflection curve. In addition, the construction histories of two buildings were evidently different. SWFC took about 10 years from 1997 to 2007 to complete its super-structure and embedments. SCT started from 2010 to 2013 to complete its super-structure and embedments. Up to now in SCT the settlement is about 82 mm, but in podium it is heave. Thus, construction engineers and design engineers should improve the design and construction. Indeed, it is not easy to explain the

unique characteristics at SWFC and SCT. Anyway according to our engineering experience it is safe for building, we could predict it by making a concrete analysis of a concrete problem in practice.

Another big problem during excavation construction is the leaks happened by settlement behind the diaphragm walls with deep excavation. For example, the deep of 31.2 m in SCT, due to certain problem, the serious leaks had occurred. Therefore, we should predict the effecting zone and the measures should be taken (adopted) before construction.

6. Discussions

6.1 Deformation of Diaphragm and Adjacent Soldier Pile

Differential settlement is the primary factor to use in evaluating the TDM. During the 1990s, diaphragm walls often leaked, and the inward displacements of diaphragm walls were larger. For example, in a 66-story building with an area of approximately 25,000 m^2 and an embedment depth of 18.20 m, the displacement due to water leakage was 99.9 mm. If engineers analyze and trace the changing deformation curve along the diaphragm wall through time, such events can most likely be avoided.

In theory, the computed deformations of diaphragm walls and soldier piles consist of heave, whereas in practice the deformations consist of settlement. Therefore, the differential deformation between a wall and an adjacent soldier pile will be larger than that between the soldier piles (Table 14).

We conclude, based on the comparisons of the computed and measured results, that the theory of interactions between the superstructure, the diaphragm wall, the piles and the soil used in TDM construction is valid and provides reasonable results in practice.

6.2 Load-sharing Role

In the 1990s, we studied the role of the diaphragm wall as a loading wall (Tang, 1996) and then used the results in practice. The computed results of load sharing by the diaphragm wall of three buildings are presented in Table 20. Note that the embedment ratio of the diaphragm wall is the primary factor responsible for the load-sharing ability of the diaphragm wall. A greater embedment ratio results in a greater load-sharing ability. This relationship is readily understood.

The simple example of the buildings of the LTJ demonstrates the advantages of the TDM. These buildings consist of two tower structures that are 7 stories tall, i.e., 50 m. There is a 2-story basement with an embedment depth of 8.9 m, a piled box foundation with a height of 9.4 m and a diaphragm 16 m long. The computed parameters are listed in Table 21. The substructure elements of the box foundation are shown in Fig. 11. The figure also shows the nodal numbers of the diaphragm wall and soldier piles, which are 14, 16, 25, 27, 36, 38, 47, 49, 58, 60, 69, 71, 80, and 82. The computed results based on the use of the TDM and the piled raft (box) foundation interaction theory are presented in Table 22. The last row of Table 22 shows that the diaphragm wall can share more than 40% of the superstructure load. This conclusion, however, should be verified using measured data.

Table 20. Computed Load Sharing by Diaphragm Wall

Building	Number of stories/ depth of embedment (m)	H(m)/ [(H-D)/D]	Load sharing by diaphragm wall,%
CFM	60/18.95	32/0.69	9.8
LCXFC	37/22.4	35/0.56	9.7
LTJ	7/8.9	16/0.80	>40.0

Note: LTJ denotes the Library of Tongji University.

Table 21. Computed Parameters Based on the Method of Soil-structure Interactions

Engineering element	Elastic modulus E (kN/m^2)	Poison's ratio, μ
Soil	1.6×104	0.50
Pile	3.0×107	0.16
Diaphragm wall	3.0×107	0.16

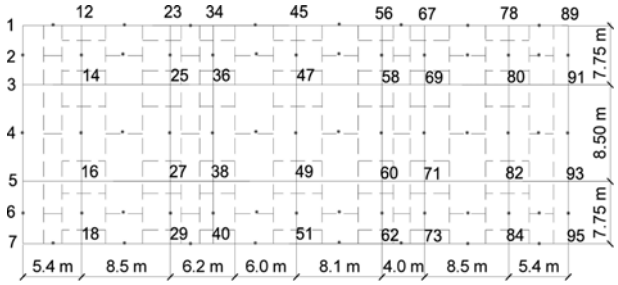

Fig. 11. Substructure Elements of the Box Foundation

Table 22. Computed Results Associated with the Use of the TDM

Number of stories of superstructure	Weight of building including box foundation (kN)	Load-sharing by soldier piles (kN)	Load-sharing by diaphragm wall (kN)
0	24,860	13,520	11,340
1	43,110	23,450	19,660
2	61,360	33,360	28,000
3	79,610	43,290	36,320
4	97,860	53,150	44,710
5	116,100	63,120	52,980
6	134,400	73,020	61,380

In addition, the embedment ratio of the diaphragm wall not only affects the load sharing by the diaphragm but also the lateral wall deflection. This ratio in Shanghai excavation engineering is typically 0.7-0.8.

For super-tall buildings with round building excavations, regardless of the depth, the maximum deformation occurs at a depth of approximately 15 m; however, this topic merits further study.

7. Conclusions

Based on the theoretical calculation and field test results for the

TDM construction mentioned above, important conclusions can be drawn, as follows:

1. Since the 1990s, we have extended the theory of soil-structure interactions to TDM construction. Currently, the technique still appears to be practical and reasonable.
2. The computed results for the CFM and LCXFC demonstrated that the use of the theory and method of superstructure-diaphragm wall-pile-foundation-soil interactions yields stress and deformation values at various stages of the process of TDM construction, particularly deformation, differential deformation, and axial forces and moments before and after raft placement, that essentially agree with the measured results.
3. The differential deformations (vertical displacements) between the diaphragm wall and the soldier pile and between the soldier piles are small, i.e., less than 20 mm and L/200, as required by the building code. These differential deformations are essentially equivalent.
4. The computed results indicated that after raft placement, the basement, including the slabs, the soldier piles and the soil, become integrated as a structural unit. By that time, the stress and strain throughout the structure have begun to be redistributed, the most evident characteristic of which is that the majority of the moments in the slabs are transferred to the raft; the calculated values essentially agree with the measurements.
5. Using the theory and the methods of superstructure-diaphragm wall-pile-foundation-soil interactions, the diaphragm wall and the loading wall can share the structural load. However, with increasing slab and structural stiffness, the structural load shared by the diaphragm wall will primarily depend on the embedment ratio.
6. The statistical-empirical formula can predict the heave of the foundation pit and lateral wall deflection, and the concept of the conservation of energy can predict the heave of the foundation pit, the lateral wall deflection and the settlement of soil behind the diaphragm wall.
7. The ratio of the lateral wall deflection and the heave in the podium to the depth of the pit far from a round excavation was greater than that near a round excavation both at the SWFC and SCT sites, which may be due to the role of the circular excavation structure in the main building. In addition, the maximum deflections occur at a depth of approximately 15 m regardless of the excavation depth. These phenomena may be unique to these cases and rare in practice, and this topic merits further theoretical study and field testing for improving design and construction.

Acknowledgements

We express our sincere thanks to Chief Engineers Fan Qinguo, Gong Jian and Deng Wenlong and to Dr. Dai Biaobing for their enthusiastic support in providing related information. We also express our thanks to Chief Engineer Xu Liping and Assistant Chief Engineer Li Tao for providing detailed information regarding the podiums of the SWFC and SCT. Financial support was provided by the National Natural Science Foundation of China (NSFC Grant No.51278359).

References

Cotton, D. M. and Luark, R. D. (2010). "Recent advances in the top-down construction of a 26.4 Meter Deep Soil Nail Retention System-Bellevue Technology Tower." *Earth Retention Conference*, pp. 375-381, DOI: 10.1061/41128(384)38.

Jia, J., Xie, X. L., Zhai, J. Q., Zhang, Y., Yang, K., and Guo, X. H. (2012). "Research and design on top-down method for large scale podium basement excavation of Shanghai Tower." *GeoCongress 2012*, pp.770-779, DOI: 10.1061/9780784412121.080.

Kim, H. J. and Mission, J. L C. (2011). "Improved evaluation of equivalent top-down load-displacement curve from a bottom-up pile load test." *J. Geotech. Geoenviron. Eng.*, Vol. 137, pp. 568-578. DOI: 10.1061/(ASCE)GT.1943-5606.0000454.

Kudsk, A., Hvam, L., Thuesen, C., Gronvold, M. B., and Olsen, M. H. (2013). "Modularization in the construction industry using a top-down approach." *The Open Construction and Building Technology Journal*, Vol. 7, pp. 88-98, DOI: 1874-8368/13.

Kung, G. T. C. (2009). "Comparison of excavation-induced wall deflection using top-down and bottom-up construction methods in Taipei silty clay." *Computers and Geotechnics*, Vol. 36, pp. 373-385, DOI: 10.1016/j.compgeo.2008.07.001.

Lee, H. S, Lee, J. Y., and Lee, J. S. (1999). "Nonshored form work system for top-down construction." *J. Constr. Eng. Manag.*, Vol. 125, No. 6, pp. 392-399, DOI: 10.1061/(ASCE)0733-9364(1999) 125:6(392).

Mana, A. L. and Clough, G. W. (1981). "Prediction of movements for braced cuts in clay." *Journal of the Geotechnical Engineering Division*, Vol. 107, No. 6, pp. 759-777.

Ministry of construction of P. R. of China (2002). GB 5007-2002. *Code for design of building foundation*, China Architectural and Building Press: Beijing (in Chinese).

Park, R. and Pauley, T. (1975). *Reinforced concrete structures*, John wiley & sons, New York.

Rhim, H. C., Kim, K. M. and Kim, S. W. (2012). "Development of an optimum pre-founded column system for top-down construction." *Journal of Civil Engineering and Management*, Vol. 18, No. 5, pp. 735-743, DOI: 10.3846/13923730.2012.723397.

Tan, Y. and Li, M. W. (2011). "Measured performance of a 26 m deep top-down excavation in downtown Shanghai." *Can. Geotech. J.*, Vol. 48, pp. 704-719, DOI: 10.1139/T10-100.

Tan, Y. and Wang, D. L. (2013). "Characteristics of a large-scale deep foundation pit excavation by the central-island technique in Shanghai soft clay. II: Top-down construction of the central construction of the peripheral rectangular pit." *Journal of Geotechnical and Geoenvironmental Engineering*, Vol. 139, pp. 1894-1910, DOI: 10.1061/(ASCE)GT.1943-5606.0000929.

Tang, M. X. (1996). *Super-structure-piled raft (box) foundation interaction with loading diaphragm wall for tall buildings*, Tongji University: Shanghai (in Chinese).

Tang, Y. J. (1996). *Theory and practice of pop-down method for tall buildings*, Tongji University: Shanghai. (in Chinese)

Tang, Y. J. and Zhao, X. H. (2014). "121-story Shanghai Center Tower foundation re-analysis using a compensated pile foundation theory." *Structural Design of Tall and Special Buildings*, Vol. 23, No. 11, pp. 854-879. DOI: 10.1002/tal.1087.

Tang, Y. J. and Zhao, X. H. (2015). "Deformation of compensated piled raft foundations with deep embedment in super-tall buildings of Sahnghai." *Structural Design of Tall and Special Buildings*, Vol. 24, No. 7, pp. 521-536.

Wang, Y. G. (2011). *Design and case studies for top-down method construction*, China Architectural and Building Press. Beijing (in Chinese).

Wang, X. J. (2014). *Deformation characteristics of Shanghai Tower podium pit and analysis of basin excavation technique*, Tongji University (in Chinese).

Xu, Z. J. and Zhao, X. H. (2002). *New development of design theory for excavation engineering-design and construction for top-down method*, China Machine Press, Beijing (in Chinese).

Zhao, X. H. (1998). *Theory of design of piled raft & piled box foundations for tall buildings in Shanghai*, Tongji University Press, Shanghai.

Zhao, X. H. (1999). *Theory of design and practice of superstructure and foundation interaction with podium*, Tongji University Press, Shanghai (in Chinese).

Zhao, X. H., Gong, J., Zhuang, B. L., Xiao, J. H., Tang, Y. J., and Zhou, H. (2014). *Comprehensive research of field test for piled raft foundation in shanghai world financial center with101-story*, China Architectural and Building Press: Beijing (in Chinese).

Zhao, X. H., Zhang, Q. H., Zhang, B. L., and Wang, Y. G. (1999). "A theory of soil-structure interaction and its application to design and construction of TDM." *J.Architecture Technology*, Vol. 30, No. 11, pp. 769-772 (in Chinese).